Resonant second-harmonic generation in a ballistic graphene transistor with an ac-driven gate

Y. Korniyenko, O. Shevtsov, and T. Löfwander
Department of Microtechnology and Nanoscience, MC2, Chalmers University of Technology, SE-412 96 Göteborg, Sweden
(Received 10 June 2015; revised manuscript received 4 January 2016; published 20 January 2016)

We report a theoretical study of time-dependent transport in a ballistic graphene field effect transistor. We develop a model based on Floquet theory describing Dirac electron transmission through a harmonically driven potential barrier. Photon-assisted tunneling results in excitation of quasibound states at the barrier. Under resonance conditions, the excitation of the quasibound states leads to promotion of higher-order sidebands and, in particular, an enhanced second harmonic of the source-drain conductance. The resonances in the main transmission channel are of the Fano form, while they are of the Breit-Wigner form for sidebands. For weak ac drive strength Z_1, the dynamic Stark shift scales as Z_1^4, while the resonance broadens as Z_1^2. We discuss the possibility of utilizing the resonances in prospective ballistic high-frequency devices, in particular frequency doublers operating at high frequencies and low temperatures.

DOI: 10.1103/PhysRevB.93.035435

I. INTRODUCTION

Already in the early years of graphene research, analog high-frequency electronics was recognized as a potential niche for applications [1–4]. Although many devices have probably been limited by parasitics due to problems with developing good recipes for making graphene transistors, the current speed record [5] is already a cutoff frequency of over 400 GHz. At the same time, we have seen a rapid improvement of graphene material quality. Mobilities reaching 10^5 cm^2/V s at room temperature and larger than 10^6 cm^2/V s at low temperature have been achieved [4]. Promising paths towards improved mobility include encapsulation of graphene between layers of other two-dimensional (2D) crystals, notably hexagonal boron nitride, or suspension of graphene between contacts. Using the latter approach, ultrahigh-quality *p-n* junctions were recently made [6]. Fabry-Perot resonances at zero magnetic field were measured, and so-called snake states were possible to see at small magnetic fields of order 20 mT. With such rapid improvements of device quality, it has become increasingly important to study in detail ballistic high-frequency devices.

One of the key ideas behind using 2D materials for high-frequency electronics is the favorable scaling towards short gate lengths without so-called short-channel effects [1]. Thin channels (2D is the extreme) allow for short gates, high speed, and high-density integration. High speed, reaching THz frequencies [7], is the ultimate goal. Another advantage of graphene is the possibility of tuning the electron density, for instance by means of a back gate: the Fermi energy can be tuned from the electron to the hole band (through the so-called Dirac point at charge neutrality). Such ambipolarity is very advantageous, in that both *n*-type and *p*-type devices can in principle be made at will across a single wafer.

A challenge is to capitalize on the unique properties of graphene and derive device functionality directly from the fact that electrons in graphene behave like massless Dirac particles with linear spectrum and a pseudospin degree of freedom. Several works in this direction show indeed that ac transport in graphene is a rich subject. Studies include quantum pumping [8–12], nonlinear electromagnetic response [13–18], and photon-assisted tunneling phenomena [19–25]. In theoretical investigations for low doping (Fermi energy E_F close to the Dirac point) and high frequencies Ω, with E_F and Ω of comparable magnitude (we put $\hbar = 1$), a true quantum mechanical description becomes necessary. For time-dependent transport in two-dimensional electron gases (2DEGs) in semiconducting heterostructures, displaying a quadratic dispersion relation, photon-assisted tunneling in time-harmonic potentials is described well within a Floquet theory framework and have been investigated for a long time [26–29]. Here, we study theoretically a ballistic field effect transistor with a harmonic drive applied to the top gate, see Fig. 1(a), within a Floquet theory applicable to graphene. The harmonic drive of frequency Ω supports inelastic scattering from the Fermi energy E_F, to sideband energies $E_n = E_F + n\Omega$, where n is an integer. Near charge neutrality, on the scale of the drive frequency, the barrier is close to transparent due to Klein tunneling. At the same time, a quasibound state on the barrier can be inelastically excited through a resonant process (supported by the harmonic drive) that interferes with direct elastic transmission. This leads to a Fano resonance in direct transmission, as recently found numerically [23–25]. Analogous Fano resonances were earlier studied [26] for few-channel waveguides in 2DEGs with attractive point scatterers (for a review of Fano resonances in nanostructures, see Ref. [30]). For graphene, the ambipolar band structure guarantees the existence of a bound state and resonances for both attractive and repulsive scatterers of arbitrary strength [see Eq. (B9) in Appendix B]. In this paper, we show that higher-order sidebands are resonantly enhanced simultaneously as the Fano resonance in direct transmission develops. This leads to the possibility of building a frequency doubler based on a ballistic graphene device that we study in detail.

The paper is organized as follows. In Sec. II we specify the model assumptions and outline the main steps in the calculation. In Sec. III we present results for the electron transmission functions for inelastic scattering at the barrier from incidence energies E to outgoing sideband energies E_n. We also analyze in detail the above mentioned resonances. In Sec. IV we present results for the dc and ac conductances, with a focus on the second ac harmonic that can be resonantly enhanced. In Sec. V we discuss in detail the dynamic Stark shift (resonance shift) and how it scales with the drive strength. In Sec. VI we summarize the paper. Finally, the appendices

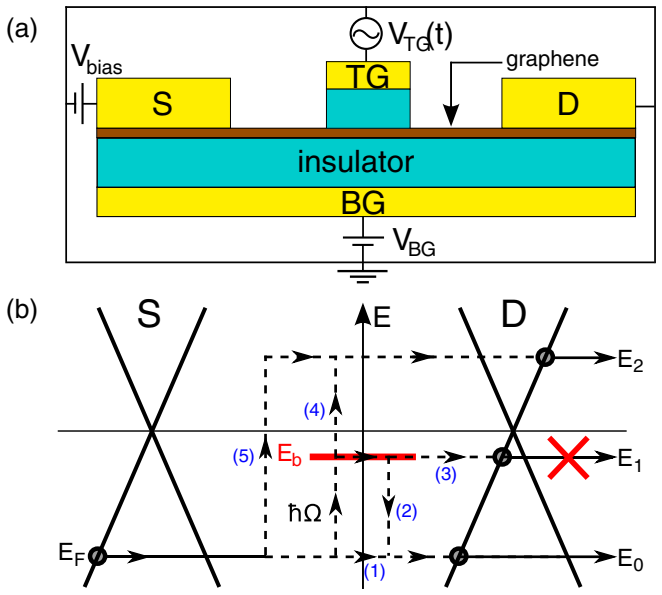

FIG. 1. (a) A graphene field effect transistor, where the overall doping level is controlled by a back gate (BG), and the source (S)–drain (D) current is controlled by the top gate (TG) dc and ac signals. (b) The harmonic ac signal of frequency Ω leads to inelastic scattering that under resonance conditions excites an otherwise unoccupied bound state in the top gate barrier potential at energy E_b. This leads to a Fano resonance in the transmission to E_0 due to interference between processes (1) and (2) and a Breit-Wigner resonance in the transmission to E_2 [process (4)]. Process (4) leads to higher-harmonic generation, in particular the 2Ω harmonic.

contain all details of the derivation outlined in Sec. II and all formulas used to obtain the results in Secs. III and IV.

II. MODEL

We are interested in the intrinsic properties of the graphene transistor in Fig. 1(a), and neglect parasitics. This allows us to make a minimal model in terms of a Dirac Hamiltonian

$$\mathcal{H} = -i\sigma_x \nabla_x + \sigma_y k_y + [Z_0 + Z_1 \cos(\Omega t)]\delta(x), \qquad (1)$$

where we have set the Fermi velocity in graphene equal to unity, $v_F = 1$. The Pauli matrices are as usual denoted σ_x and σ_y. The top gate barrier potential is considered smooth on the atomic scale and cannot induce scattering between the two valleys in the band structure. In the end all observables will contain an extra factor of 2 to account for valley degeneracy, in addition to spin degeneracy. At the same time, on the Dirac length scale (given by $\hbar v_F/E_F$ after reinstating $\hbar$ and v_F), we consider the potential width D to be small but its height V to be large, such that we can take the limits $D \to 0$ and $V \to \infty$ keeping the product $VD = Z$ constant. The strengths of the time-independent component Z_0 and the time-dependent component Z_1 can be different. The δ function in Eq. (1) is therefore smooth on the atomic scale but sharp on the Dirac length scale. We consider the barrier to be translationally invariant along the transverse direction, which guarantees that the corresponding wave vector component k_y is conserved. The spatial dependence then enters through the coordinate x perpendicular to the barrier. We assume homogeneous doping of the graphene sheet tuned by the back gate and that source and drain contacts are sufficiently far away from the barrier that evanescent waves from the contacts can be neglected; i.e., we avoid in this paper the so-called pseudodiffusive limit [31].

The methodology to solve the problem at hand is to first solve the scattering problem for the wave functions satisfying the Dirac equation

$$\mathcal{H}\psi(x,k_y,t) = i\,\partial_t \psi(x,k_y,t). \qquad (2)$$

The solution can be collected into a unitary scattering matrix for reflection and transmission coefficients between incoming waves at energy E and scattered waves at energies $E_n = E + n\Omega$. For the current, the Landauer-Büttiker approach [32] is used to compute the current operator in terms of creation and annihilation operators for incoming and scattered waves, where the latter are related to the former through the scattering matrix. A statistical average is performed to obtain the time-dependent current that depends on the occupation factors of the source and drain leads, which are given by the Fermi function with chemical potentials shifted by the applied source-drain voltage eV. Below, we shall give results for the conductance in linear response to the applied source-drain voltage at zero temperature.

For the scattering problem, since the Hamiltonian is periodic in time, we use a general Floquet ansatz

$$\psi(x,k_y,t) = \sum_n \psi_n(x,k_y,E)\exp(-iE_n t). \qquad (3)$$

When plugged into Eq. (2) it yields a set of coupled differential equations for the (formally infinitely many) sideband amplitudes $\psi_n(x,k_y,E)$. In the following we do not write the arguments x, k_y, and E in order to keep the notation compact. The sideband amplitudes can be arranged into a vector $\Phi = [\ldots,\psi_{-1},\psi_0,\psi_1,\ldots]^T$, which then satisfies

$$\nabla_x \Phi = \check{M}_{td}\Phi, \qquad (4)$$

where

$$\check{M}_{td} = [k_y\sigma_z + iE_n\sigma_x - iZ_0\sigma_x\delta(x)] \otimes \check{1} - i\frac{Z_1}{2}\delta(x)\sigma_x \otimes \check{2}. \qquad (5)$$

Here, $\check{M}_{td}$ is a tridiagonal matrix in sideband space with $(\check{1})_{nm} = \delta_{nm}$ and $(\check{2})_{nm} = \delta_{n,m+1} + \delta_{n,m-1}$. After integration over $x = 0$ we obtain a boundary condition

$$\Phi(x = 0^-) = \exp\left[iZ_0\sigma_x \otimes \check{1} + i\frac{Z_1}{2}\sigma_x \otimes \check{2}\right]\Phi(x = 0^+)$$
$$\equiv \check{M}\Phi(x = 0^+). \qquad (6)$$

This boundary condition can also be derived by solving a square barrier problem first, and in the end let $D \to 0$ and $V \to \infty$ keeping the product $VD = Z$ constant; see also Ref. [33]. This boundary condition gives an elegant view of scattering off a potential in graphene in terms of pseudospin rotation. For instance, the static barrier leads to a rotation around the pseudospin x axis by an angle $-2Z_0$. If the pseudospin is aligned with σ_x, i.e., electron propagation along the x axis with perpendicular incidence, the rotation has no effect (Klein tunneling [34]). For other angles, transmission is nonperfect. The formulas for the transmission amplitudes $t_n(k_y,E)$ derived from Eq. (6) are given in Eq. (B14).

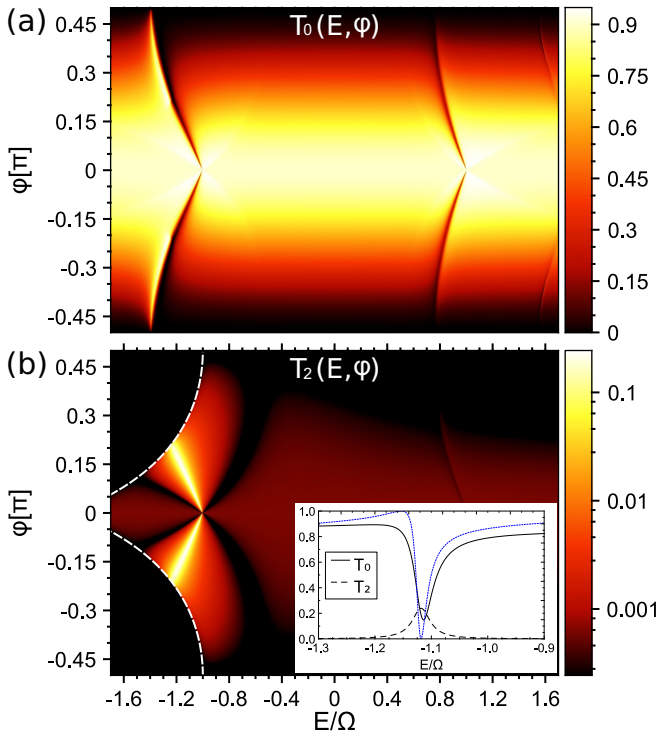

FIG. 2. Energy and incidence angle dependence of transmission probabilities for (a) elastic scattering $T_0(E,\varphi)$ and (b) inelastic scattering between energy E and $E+2\Omega$, $T_2(E,\varphi)$. The black regions to the left of the white dashed lines in (b) are regions where the second-sideband wave functions are evanescent waves decaying away from the barrier. The barrier strengths are $Z_0 = 0.4\pi$ and $Z_1 = 0.45$. Inset: Transmission probabilities for fixed $\varphi = \pi/9$.

III. TRANSMISSION AMPLITUDES

In Fig. 2 we display the transmission probabilities $T_n(E,\varphi) = |t_n(E,\varphi)|^2$ for $n = 0$ and $n = 2$, where $T_n(E,\varphi)$ denotes incidence on the barrier at energy E and transmission at sideband energy E_n, keeping the parallel momentum $k_y = |E|\sin\varphi$ conserved (the angle φ is measured relative to the barrier normal). In the main transmission channel $T_0(E,\varphi)$, Klein tunneling is apparent in that the transmission is very close to unity. Deviation from unity transmission is due to the static barrier of strength Z_0 and finite incidence angle (nonzero φ) and, in addition, scattering to other sidebands with $n \neq 0$. The transmission probability to the second sideband $T_2(E,\varphi)$ is in general very small. For certain energies there are Fano resonances [23–25] induced by the time-dependent drive and a bound state at the barrier, which give rise to a peak-dip structure dispersing with φ, one feature at positive energies and another one at negative energies. The Fano resonances occur in a parameter range where the outgoing waves (from the barrier) at a sideband E_n are evanescent (below we shall concentrate on $n = \pm 1$, which are the most pronounced resonances in Fig. 2). This happens when inelastic scattering from $E^2 = k_x(E)^2 + k_y^2$ to $E_n^2 = k_x(E_n)^2 + k_y^2$ (with conserved k_y) causes $k_x(E_n)$ to become imaginary. Resonant behavior occurs due to the existence of a bound state on the barrier at energy $E_b(Z_0,k_y) = -\mathrm{sgn}(Z_0)|k_y|\cos Z_0$ [cf. Eq. (B9)] that can be excited by the ac drive (in which case it becomes quasibound). The Fano resonance at $E_r = E_b \pm \Omega$ is a quantum mechanical interference between direct elastic tunneling and a tunneling process involving excitation to the first sideband (for $n = \pm 1$ at $E_r = E_b \mp \Omega$) and deexcitation back to energy E; see paths (1) and (2) in the diagram in Fig. 1(b) for the $E < 0$ case. On resonance, inelastic tunneling to the second sideband is enhanced and $T_{\pm 2}(E,\varphi)$ display Breit-Wigner resonance peaks at $E_r = E_b \mp \Omega$; see Fig. 2(b). The resonance in $T_2(E,\varphi)$ can be viewed as due to transmission in energy space through a double barrier structure with barrier heights proportional to Z_1.

To extract more information about the above numerical results, we proceed with an analytic approximation. We can expand the boundary condition in Eq. (6) to second order in the ac drive strength Z_1, assuming $Z_1 \ll 1$,

$$\check{M} \approx e^{iZ_0\sigma_x}\left[\check{1} + \frac{iZ_1}{2}\sigma_x \otimes \check{2} - \frac{Z_1^2}{8}(2\cdot\check{1} + \check{3})\right], \qquad (7)$$

where $(\check{3})_{nm} = \delta_{n,m+2} + \delta_{n,m-2}$ in sideband space. To second order in Z_1, the transmissions to the first two sidebands can be computed by solving a system of equations for t_0, $t_{\pm 1}$, and $t_{\pm 2}$; see Appendix C. We separate two cases: (i) off-resonant transmission and (ii) on-resonant transmission. For case (i) off-resonant transmission, the equation system can be inverted directly and we get (for each φ; we suppress the argument φ below for brevity)

$$\begin{aligned} t_0(E) &\approx \Big[1 + \frac{Z_1^2}{4} + Z_1^2 t^{(0)}(E)A_{0,1}(E)t^{(0)}(E_1)A_{1,0}(E) \\ &\quad + t^{(0)}(E)A_{0,-1}(E)t^{(0)}(E_{-1})A_{-1,0}(E)\Big]t^{(0)}(E), \\ t_{\pm 1}(E) &\approx -Z_1 t^{(0)}(E_{\pm 1})A_{\pm 1,0}(E)t^{(0)}(E), \\ t_{\pm 2}(E) &\approx Z_1^2[t^{(0)}(E_{\pm 2})A_{\pm 2,\pm 1}(E)t^{(0)}(E_{\pm 1})A_{\pm 1,0}(E) \\ &\quad - t^{(0)}(E_{\pm 2})A_{\pm 2,0}(E)]t^{(0)}(E), \end{aligned} \qquad (8)$$

where $t^{(0)}(E_n)$ is the transmission amplitude without ac drive computed at energy E_n, and $A_{n,m}(E)$ is a transition amplitude in energy space between energies E_m and E_n, which can be related to off-diagonal matrix elements (in sideband space) of the matrix $\check{M}$ in Eq. (7). The above expressions make the inelastic tunneling processes at play explicit, see enumerated processes in Fig. 1(b). For instance, the expression for $t_1(E)$, read from right to left, has a transparent physical meaning. It consists of transmission amplitudes at E and E_1, separated by a transition in energy space $A_{1,0}$, corresponding to absorption of one quantum Ω. Consequently, the process is of order Z_1. Direct transmission has corrections to the static transmission amplitude due to excitation and deexcitation to neighboring sidebands (processes of order Z_1^2), while $t_2(E)$ consists of a direct process of absorbing two quanta, 2Ω, and a sequential process involving the first-sideband energy; both are of order Z_1^2. This tells us that the sideband amplitudes are in general very small when Z_1 is small.

The above picture changes for case (ii) on-resonant transmission, for energies near $E_r = E_b \pm \Omega$ [we shall concentrate on $E_b - \Omega$ in the following discussion, as in Fig. 1(b)]. In this case, the equation determining the function $t^{(0)}(E_n,k_y)$ at energy $E_n = E_b$ (here $n = 1$) has to be reconsidered. There is a

pole in the matrix equation determining the scattering matrix at this energy for fixed k_y, corresponding to formation of a bound state with evanescent waves decaying away from the barrier. The bound state is unoccupied (decoupled from reservoirs) in the absence of the ac drive. For case (ii) on-resonant transmission, we get for energies δE around the resonance energy E_r

$$t_0(E_r+\delta E) \approx \frac{\delta E - Z_1^2 h_2(E_r)}{\delta E + i Z_1^2 h_1(E_r)} t^{(0)}(E_b), \tag{9}$$

$$t_2(E_r+\delta E) \approx \frac{Z_1^2 h_3(E_r)}{\delta E + i Z_1^2 h_1(E_r)} t^{(0)}(E_b+2\Omega), \tag{10}$$

where $h_j(E_r) \equiv h_j(E_r,k_y,Z_0)$, $j=1,2,3$, are complex-valued functions that can be read off from Eqs. (C9) and (C10) [their explicit forms are not important in the discussion below, except to note that $h_1(E_r)$ is purely real]. Note that t_1 is not well defined near resonance (it was eliminated in the calculation) because it is related to the excitation of the bound state. The conductance computed below will not get contributions from this sideband energy [crossed process (3) in Fig. 1(b)]. For the direct transmission probability $T_0(E_r+\delta E)$, neglecting for a while the second-sideband contribution (setting $h_2=0$ above), there is a characteristic Fano resonance form $T_0(E_r+\delta E) \propto (q\Gamma/2+\delta E)/[\delta E^2+(\Gamma/2)^2]$, where $\Gamma \propto Z_1^2\Omega$ and q is of order unity, $O[(Z_1)^0]$. This is the blue dotted line displayed in the inset of Fig. 2(b). Taking into account tunneling (in energy space) to the second sideband (h_2 finite above) and higher, we obtain the corrected line shape, the black solid line in the inset of Fig. 2(b). For the probability to scatter inelastically to the second sideband, we obtain from the above a Breit-Wigner resonance with the characteristic form $T_2(E_r+\delta E) \propto (\Gamma/2)/[\delta E^2+(\Gamma/2)^2]$, which is displayed as the black dashed line in the inset of Fig. 2(b). Thus, in a range $\delta E \propto Z_1^2\Omega$ around E_r, the response is highly nonlinear and higher-order harmonics can be resonantly enhanced, in particular the second harmonic.

IV. DC AND AC CONDUCTANCES

To quantify the resonant generation of the second harmonic, we present calculations of the linear conductances G_n, both the time-averaged component ($n=0$) in Fig. 3 and the first two harmonics ($n=1$, 2) in Fig. 4. Note that in the linear response (small source-drain voltage), the source-drain ac current $I=\sum_n I_n e^{-in\Omega t}$, with its harmonics I_n, naturally defines ac conductance components G_n; see Appendix D. In Fig. 3(a) we plot the angle resolved conductance $G_0(E_F,\varphi)$, which reflects the sum over transmission functions, including the ones displayed in Fig. 2. After angle integration, we obtain the dc linear conductance; see the solid black line in Fig. 3(b). Due to the ac drive, the dc conductance contains features not present in the static case (included as thin green straight lines). The Fano resonance is clearly visible as a peak-dip feature in $G_0(E_F)$. Thus, it is enough to study the time-averaged conductance to infer influence of the ac drive.

In Fig. 4 we present the real and imaginary parts of the first and second harmonics, $G_1(E_F)$ and $G_2(E_F)$. For small drive amplitude Z_1, the harmonics generally scale as Z_1^n in perturbation theory and the second harmonic is expected to

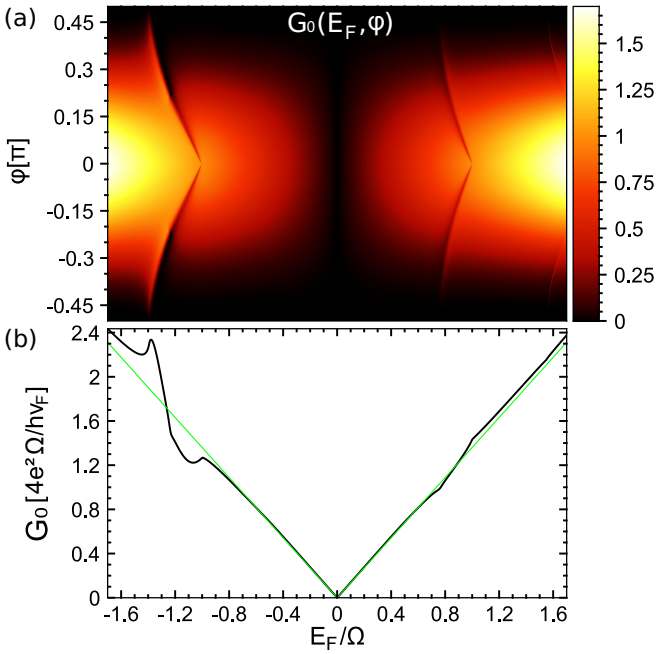

FIG. 3. Zero-temperature source-drain dc linear conductance in the presence of ac drive of strength $Z_1=0.45$ on the top gate. Upper panel: Impact angle resolved dc conductance $G_0(E_F,\varphi)$. Lower panel: Angle integrated time-average dc conductance $G_0(E_F)$ (black solid line). The green straight line is $G_0(E_F)$ in the static case, $Z_1=0$, for comparison. The dip-peak structures are related to the Fano and Breit-Wigner resonances in the elastic and inelastic transmission functions. The static barrier strength is $Z_0=0.4\pi$.

be small. Near resonance, however, it is enhanced to order unity, $O[(Z_1)^0]$, within a window of doping $\sim Z_1^2\Omega$ around $E_F=E_r$. This results in the second harmonic becoming of the same magnitude as the first harmonic already for weak driving ($Z_1=0.45$ in the figure). This leads us to the conclusion that the device can operate as a frequency doubler.

Parameter regimes

Parameter regimes available experimentally will affect the possibility of measuring frequency doubling. First we discuss typical gate lengths and drive amplitudes. These two quantities are connected by the dimensionless parameter $Z_1=V_1 D/\hbar v_F$ (reinstating $\hbar$ and v_F). For graphene, $v_F \sim 10^6$ m/s. For gate lengths of order 100 nm, we obtain a drive amplitude of $V_1 \sim 6Z_1$ meV. For relatively weak driving as considered above, $Z_1 \sim 1$, the required drive amplitude is a few meV, which is reasonable [35]. If the source is weaker, the gate length has to be increased. Typical gate lengths used in experiments today are of order 1 μm, which with the help of nanowires have been brought down to 170 nm [36].

Until today, graphene devices operating at room temperature display frequency doubling in the frequency range 1–10 GHz [36]. Their operating principle is classical, only relying on the bipolar gate voltage dependence of the dc conductance [see thin green line in Fig. 3(b)]. With the Fermi energy at dc operation aligned to the conductance minimum, for instance by applying a suitable back gate voltage V_{BG}, an additional ac signal with frequency Ω on

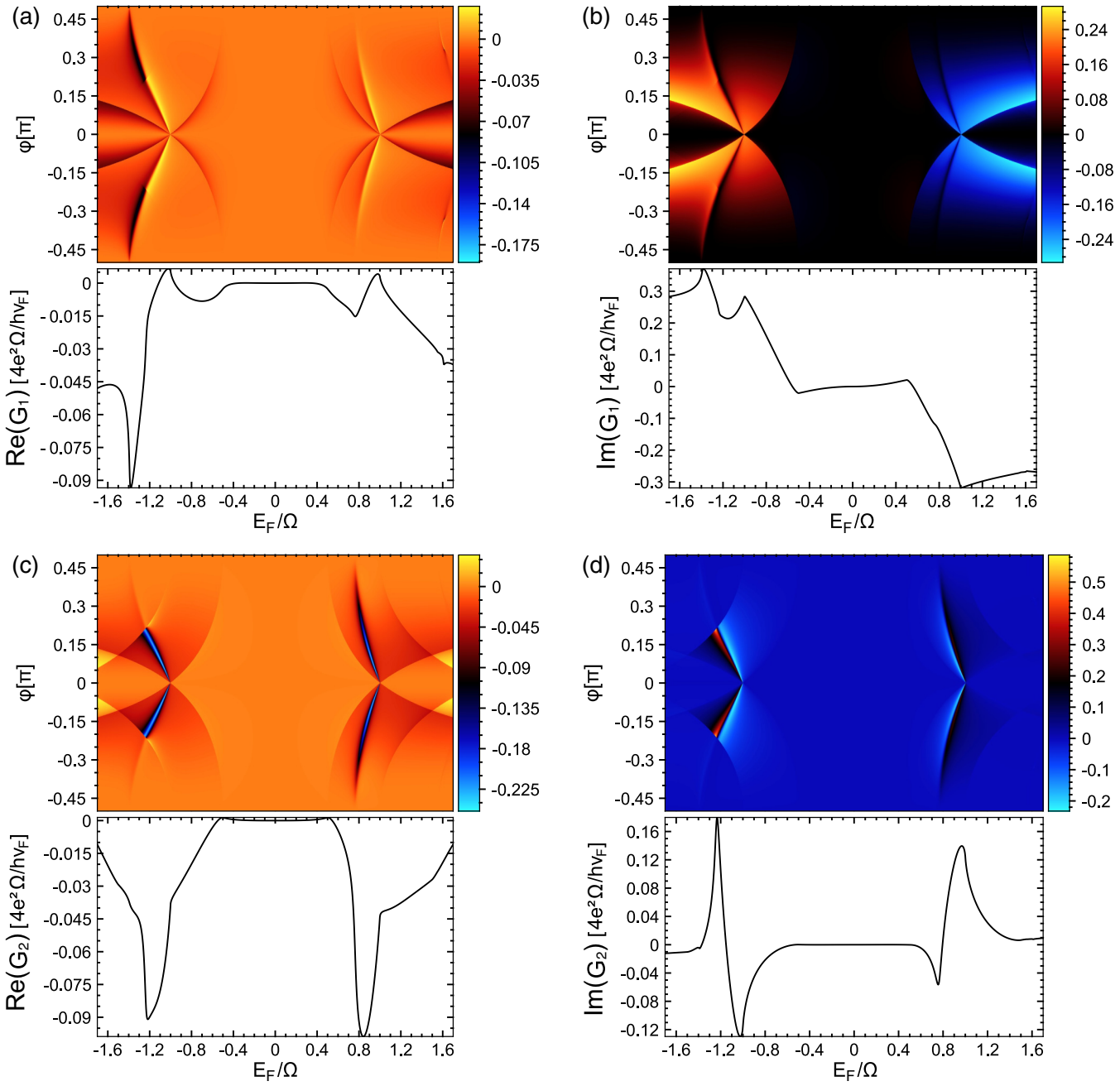

FIG. 4. Zero-temperature source-drain linear conductances for sideband currents with $n = \pm 1$ and $n = \pm 2$ in the presence of an ac drive of strength $Z_1 = 0.45$ on the top gate. Upper panels: Impact angle resolved average conductances $G_n(E_F,\varphi)$. Lower panels: Angle integrated real and imaginary parts of average conductances $G_n(E_F)$. The static barrier strength is $Z_0 = 0.4\pi$.

the top gate (locally modulating the Fermi energy) leads to a source-drain conductance response at frequency 2Ω simply because $G(-E_F) = G(E_F)$. For our proposed device, on the other hand, the operating principle is based on a quantum mechanical resonance effect. For weak driving, low temperature is therefore needed. For $Z_1 \ll 1$, the resonance width scales as $Z_1^2\hbar\Omega$. To avoid broadening, we must require small temperature $k_BT \ll Z_1^2\hbar\Omega$. For a frequency of order 50 GHz we get $T \sim 2$ K for $Z_1 \sim 1$. For stronger drive, this constraint is less restrictive. It remains to be experimentally explored whether also room temperature operation and higher frequency, 100 GHz to 1 THz, are possible to achieve for stronger driving in a ballistic device. We note that another quantum effect, the quantum Hall effect, has been observed at room temperature in graphene devices [37].

V. DYNAMIC STARK SHIFT

As we have seen above, in the presence of the ac drive, the barrier-induced bound state is excited and appears as a quasibound state, which is broadened as well as shifted in energy with respect to the original bound state. This dynamic Stark shift can be investigated quantitatively by computing the determinant of the matrix $\mathbf{M}_s$ defined in

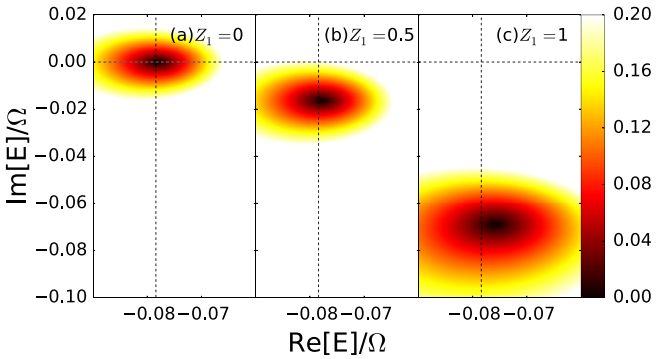

FIG. 5. Dynamic Stark shift as illustrated by plotting det[$\mathbf{M_s}$] as a function of complex energy E, where the matrix $\mathbf{M_s}$ is defined in Eq. (B16). The points $E_{\rm zero}$ in the complex energy plane where this function vanishes coincide with resonances in the Floquet scattering matrix. (a) Without the ac drive, $Z_1 = 0$, there is a true bound state and the determinant vanishes at $\mathrm{Re}[E] = E_b$ and $\mathrm{Im}[E] = 0$. (b) and (c) Including the ac drive, $Z_1 > 0$, the minimum moves out into the complex plane. The dashed lines indicate the position of the bound state in the absence of the ac drive. The static barrier strength is $Z_0 = 0.4\pi$ and the impact angle is $\varphi = \pi/9$.

Eq. (B16). In the absence of driving, the matrix is diagonal with the nth matrix element given by $D(k_y, E_n)$; cf. Eq. (B4). The determinant therefore vanishes, $\det[\mathbf{M_s}] = 0$, if one of the sideband energies equals the bound state energy E_b, since $D(k_y, E_n = E_b) = 0$ as explained in Appendix B 2. Including drive, $Z_1 > 0$, the zeros of the determinant move into the complex energy plane [26,38], $E_b \to E_{\rm zero}$, signaling a quasibound state. The resonance energy $E_r = \mathrm{Re}(E_{\rm zero})$ is then shifted from E_b. The resonance width can be related to $\mathrm{Im}(E_{\rm zero})$. This effect is illustrated in Fig. 5, where we plot $\det[\mathbf{M_s}]$ as function of complex energy. In Fig. 6 we plot the resonance energy shift and the broadening as a function of drive strength. For weak drive, the shift is proportional to $Z_1^4\Omega$, while the broadening scales as $Z_1^2\Omega$. For stronger drive, higher-order contributions lead to a deviation from this scaling. The resonance shift could be mapped out directly in an experiment, since the Fermi energy of graphene is tunable by the back gate.

VI. SUMMARY

In summary, we have investigated time-dependent transport in a ballistic graphene field effect transistor with ac drive on its top gate. We find resonances in inelastic scattering to sideband energies related to excitation of a quasibound state in the top gate barrier. This leads to substantial resonant enhancement of the second harmonic of the source-drain conductance, that could possibly be used in developing a frequency doubler based on a ballistic device.

ACKNOWLEDGMENTS

It is a pleasure to thank V. S. Shumeiko and J. Stenarson for valuable discussions. We acknowledge financial support from the Swedish Foundation for Strategic Reseach (SSF) and the Knut and Alice Wallenberg Foundation (KAW).

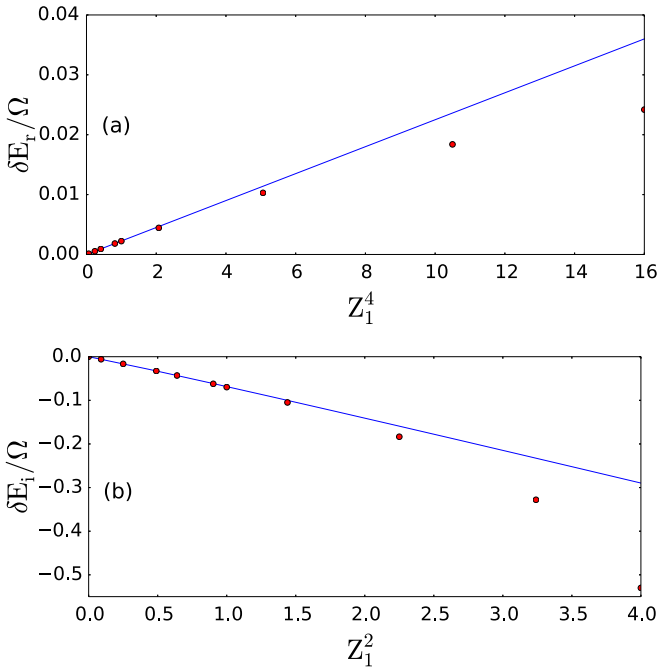

FIG. 6. (a) The dynamic Stark shift scales with the drive strength as Z_1^4 for small Z_1. (b) The broadening scales as Z_1^2. The static barrier strength is $Z_0 = 0.4\pi$ and the impact angle is $\varphi = \pi/9$.

APPENDIX A: WAVE SOLUTIONS IN GRAPHENE

1. General solution

We start by introducing general wave solutions in graphene without time-dependent perturbation. They are known (see, e.g., Refs. [39,40]) and we write them down here to establish a coherent notation for subsequent sections. As mentioned in the main text, we consider only one valley (one K point) described by the Hamiltonian

$$\mathcal{H}_0 = -i\boldsymbol{\sigma}\cdot\nabla, \quad \boldsymbol{\sigma} = (\sigma_x, \sigma_y). \tag{A1}$$

We have to solve the Dirac equation $i\partial_t\psi(x,y,t) = \mathcal{H}_0\psi(x,y,t)$, which is done by the standard ansatz

$$\psi(x,y,t) \propto e^{ik_x x}e^{ik_y y}e^{-iEt}\psi(k_x,k_y,E). \tag{A2}$$

We obtain the following eigenvalues and eigensolutions,

$$E_\lambda(k_x,k_y) = \lambda\sqrt{k_x^2+k_y^2}, \quad \lambda = \pm 1, \tag{A3}$$

$$\psi_\lambda(k_x,k_y,E) = \frac{1}{\sqrt{2}}\begin{pmatrix} 1 \\ \frac{k_x+ik_y}{E_\lambda} \end{pmatrix}. \tag{A4}$$

2. Scattering basis

Note that once we have found the spectrum, Eq. (A3), there are only two independent parameters labeling eigenstates, e.g., (k_x,k_y) or (k_y,E). Since we are going to build a scattering theory following Büttiker [32,41] the latter choice is natural because we assume translational invariance along the barrier (y axis); cf. Eq. (1). In order to introduce the scattering basis we have to find the group velocity of states propagating along the x axis (perpendicular to the barrier). Using standard definitions

we have

$$u(k_y,E)=\frac{\partial E}{\partial k_x}=\pm v(k_y,E),$$
$$v(k_y,E)=\frac{\kappa_x(k_y,E)}{E},\tag{A5}$$
$$\kappa_x(k_y,E)=\mathrm{sgn}(E)\sqrt{E^2-k_y^2},$$

where the upper and lower signs describe particles moving in the positive and negative directions along x, respectively. Then we can introduce a scattering basis via

$$\psi_{\rightarrow}(x,k_y,E)=\frac{1}{\sqrt{2v(k_y,E)}}\begin{pmatrix}1\\ \eta(k_y,E)\end{pmatrix}e^{i\kappa_x(k_y,E)x},$$
$$\psi_{\leftarrow}(x,k_y,E)=\frac{1}{\sqrt{2v(k_y,E)}}\begin{pmatrix}1\\ \bar{\eta}(k_y,E)\end{pmatrix}e^{-i\kappa_x(k_y,E)x},\tag{A6}$$
$$\eta(k_y,E)=\frac{\kappa_x(k_y,E)+ik_y}{E},$$
$$\bar{\eta}(k_y,E)=\frac{-\kappa_x(k_y,E)+ik_y}{E},$$

where arrows indicate the direction of propagation. The normalization in Eq. (A6) is chosen such that particles carry unit probability flux along the x axis, defined as

$$j_x(x,k_y,E)=\psi^{\dagger}(x,k_y,E)\sigma_x\psi(x,k_y,E).\tag{A7}$$

This basis is used to find a scattering matrix and build the scattering field theory below.

APPENDIX B: FLOQUET SCATTERING MATRIX IN GRAPHENE WITH AC δ POTENTIAL

Let us now discuss the Floquet scattering matrix for graphene in the presence of an oscillating line scatterer; i.e., we consider a system described by [cf. Eq. (1)]

$$\mathcal{H}=\mathcal{H}_0+[Z_0+Z_1\cos(\Omega t)]\delta(x).\tag{B1}$$

Before discussing the solution associated with the full time-dependent Hamiltonian, it is instructive to consider the stationary case, $Z_1=0$.

1. Static δ barrier

For a static barrier, scattering is elastic, and it is easy to write down a scattering ansatz, first assuming incoming particles from the left,

$$\psi(x,k_y,E)=\begin{cases}\psi_{\rightarrow}(x,k_y,E)+r^{(0)}\psi_{\leftarrow}(x,k_y,E), & x<0,\\ t^{(0)}\psi_{\rightarrow}(x,k_y,E), & x>0.\end{cases}\tag{B2}$$

The superscript $X^{(0)}$ indicates functions X computed for a static barrier. The unknown transmission $t^{(0)}(k_y,E)$ and reflection $r^{(0)}(k_y,E)$ coefficients are found through the boundary condition at $x=0$, which reads [cf. Eq. (6)]

$$\psi(0^-,k_y,E)=\exp[iZ_0\sigma_x]\psi(0^+,k_y,E).\tag{B3}$$

It is straightforward to find a solution to Eq. (B3), but it is convenient for what follows to write down an equation satisfied by $t^{(0)}$,

$$D(k_y,E)t^{(0)}=1,$$
$$D(k_y,E)=\frac{1}{2v(k_y,E)}\begin{pmatrix}-\bar{\eta}(k_y,E) & 1\end{pmatrix}\times\exp[iZ_0\sigma_x]\begin{pmatrix}1\\ \eta(k_y,E)\end{pmatrix}.\tag{B4}$$

Using Eq. (A6) we can easily simplify Eq. (B4) and obtain

$$t^{(0)}(k_y,E)=D(k_y,E)^{-1}=\left(\cos Z_0+i\frac{\sin Z_0}{v(k_y,E)}\right)^{-1}.\tag{B5}$$

Let us introduce an incidence angle φ, measured relative to the barrier normal, via $k_y=|E|\sin\varphi$. Equation (B5) can then be rewritten as

$$t^{(0)}(k_y,E)=\frac{\cos\varphi}{\cos\varphi\cos Z_0+i\sin Z_0}.\tag{B6}$$

2. Barrier-induced bound state

It is well known [42] that poles of the scattering matrix correspond to bound states. In our case the static δ barrier induces exactly one bound state as will be shown now. We equate to zero the denominator of Eq. (B5), giving

$$\kappa_x(k_y,E)=-iE\tan Z_0.\tag{B7}$$

Equation (B7) is periodic in Z_0 and we consider for definiteness $-\frac{\pi}{2}<Z_0<\frac{\pi}{2}$. We then impose a condition that the bound state solution has to be decaying away from the barrier, which means

$$\kappa_x(k_y,E)=i\sqrt{k_y^2-E^2}.\tag{B8}$$

Collecting the above, the energy of the bound state is given by

$$E_b=-\mathrm{sgn}(Z_0)|k_y|\cos Z_0.\tag{B9}$$

It is interesting to note that the bound state plays no role in dc transport in our model setup since it is disconnected from the continuum of propagating waves connecting the contacts. This circumstance changes as soon as we allow inelastic scattering on the barrier, when $Z_1\neq 0$.

3. Oscillating δ barrier

In the case when $Z_1\neq 0$ the Hamiltonian, Eq. (B1), is periodic in time, which enables us to use the Floquet theorem[27–29] for finding eigenvectors,

$$\psi(x,k_y,t)=e^{-iEt}\sum_{n=-\infty}^{+\infty}e^{-in\Omega t}\psi_n(x,k_y,E).\tag{B10}$$

We organize the (formally infinite) many sideband amplitudes $\psi_n(x,k_y,E)$ into a column vector

$$\Phi(x,k_y,E)=\begin{pmatrix}\cdots\\ \psi_{-1}(x,k_y,E)\\ \psi_0(x,k_y,E)\\ \psi_1(x,k_y,E)\\ \cdots\end{pmatrix},\tag{B11}$$

and write down the condition to be satisfied at $x = 0$ [cf. Eq. (6)],

$$\Phi(0^-,k_y,E) = \check{M}\Phi(0^+,k_y,E),$$
$$\check{M} = \exp\left[i Z_0\sigma_x \otimes \check{1} + i\frac{Z_1}{2}\sigma_x \otimes \check{2}\right], \quad \text{(B12)}$$
$$[\check{1}]_{n,m} = \delta_{n,m}, \quad [\check{2}]_{n,m} = \delta_{n,m+1} + \delta_{n,m-1}.$$

Since the barrier is active only at $x = 0$, asymptotic solutions are still given by a linear combination of the static solutions in Eq. (A6). The barrier only scatters an incident particle with quantum numbers (E,k_y) into a linear combination of states with quantum numbers (E_n,k_y). In the end, for our model, we have to consider only propagating outgoing waves, $E_n > |k_y|$, for calculating transport properties. Therefore we use the following ansatz:

$$\psi_n(x,k_y,E) = \begin{cases} \delta_{n,0}\psi_{\rightarrow}(x,k_y,E_n) + r_n\psi_{\leftarrow}(x,k_y,E_n), & x < 0, \\ t_n\psi_{\rightarrow}(x,k_y,E_n), & x > 0. \end{cases} \quad \text{(B13)}$$

We can eliminate reflection coefficients $r_n(k_y,E)$ and find a system of equations for $t_n(k_y,E)$ only, which reads

$$\sum_m \frac{1}{2\sqrt{v(k_y,E_n)v(k_y,E_m)}}(-\bar{\eta}(k_y,E_n) \quad 1) \times[\check{M}]_{nm}\begin{pmatrix}1\\ \eta(k_y,E_m)\end{pmatrix}t_m = \delta_{n,0}. \quad \text{(B14)}$$

Equation (B14) must be solved numerically, in principle for infinite number of sidebands. In practice, the number of sidebands can be limited to $n \in [-N_c,N_c]$, where the cutoff N_c can be estimated by expanding Eq. (B12) and studying the coupling to sidebands. In this way we find a tolerance measure ϵ for the cutoff,

$$\frac{(Z_1/2)^{N_c}}{[(N_c/2)!]^2} < \epsilon. \quad \text{(B15)}$$

With the sideband cutoff, the above system of equations can be collected into the matrix form

$$\mathbf{M_s}\cdot\mathbf{t} = \boldsymbol{\delta}_{n,0}, \quad \text{(B16)}$$

where $\mathbf{M_s}$ is a $(2N_c+1)\times(2N_c+1)$ matrix, $\mathbf{t}$ is a vector of length $2N_c+1$ with the transmission functions $t_n(k_y,E)$ for $n \in [-N_c,N_c]$, and $\boldsymbol{\delta}_{n,0}$ is a vector of length $2N_c+1$ with elements $\delta_{n,0}$. The transmission functions are found by inverting the matrix $\mathbf{M_s}$.

APPENDIX C: ANALYSIS OF SIDEBAND TRANSMISSION COEFFICIENTS: FANO AND BREIT-WIGNER RESONANCES

For $Z_1 \ll 1$, we expand $\check{M}$ up to terms of order $O(Z_1^2)$, and consider five outgoing channels with $n = \{0, \pm 1, \pm 2\}$. Then we obtain a system of five coupled equations which reads [omitting the arguments (k_y,E) for brevity]

$$\begin{aligned}
\left(1-\frac{Z_1^2}{4}\right)D_2t_2 + Z_1A_{2,1}t_1 + Z_1^2A_{2,0}t_0 &= 0,\\
Z_1A_{1,2}t_2 + \left(1-\frac{Z_1^2}{4}\right)D_1t_1 + Z_1A_{1,0}t_0 + Z_1^2A_{1,-1}t_{-1} &= 0,\\
Z_1^2A_{0,2}t_2 + Z_1A_{0,1}t_1 + \left(1-\frac{Z_1^2}{4}\right)D_0t_0 + Z_1A_{0,-1}t_{-1} + Z_1^2A_{0,-2}t_{-2} &= 1,\\
Z_1^2A_{-1,1}t_1 + Z_1A_{-1,0}t_0 + \left(1-\frac{Z_1^2}{4}\right)D_{-1}t_{-1} + Z_1A_{-1,-2}t_{-2} &= 0,\\
Z_1^2A_{-2,0}t_0 + Z_1A_{-2,-1}t_{-1} + \left(1-\frac{Z_1^2}{4}\right)D_{-2}t_{-2} &= 0,
\end{aligned} \quad \text{(C1)}$$

where we have used the following notations:

$$D_n(k_y,E) = D(k_y,E_n),$$
$$A_{n,m} = \frac{(i/2)^{|n-m|}}{|n-m|}\frac{1}{2\sqrt{v(k_y,E_n)v(k_y,E_m)}}(-\bar{\eta}(k_y,E_n) \quad 1) \times \exp[i Z_0\sigma_x]\sigma_x^{|n-m|}\begin{pmatrix}1\\ \eta(k_y,E_m)\end{pmatrix}, \quad n \neq m. \quad \text{(C2)}$$

Note that from Eq. (C2) and Eq. (B4) it is obvious that $D_n^{-1}(k_y,E) \equiv t^{(0)}(k_y,E_n)$ provided the corresponding wave is propagating, i.e., $E_n > |k_y|$. On the other hand the new functions $A_{n,m}$ have a meaning of transition matrix between the sidebands. Now we recall that the presence of a (static) δ barrier implies the existence of a bound state, see Appendix B 2, which now can be coupled to the propagating waves via inelastic scattering. In this case one of the functions $D_n(k_y,E)$ vanishes when $E_n = E_b$. This possibility leads to resonances in the transmission spectrum of the sidebands (see Fig. 7), as will be discussed in detail below.

1. Off-resonant transmission

We will first consider the rather trivial case of transmission in different sidebands away from the resonances. In this case we can straightforwardly estimate orders of magnitude for the sideband transmission coefficients keeping only contributions

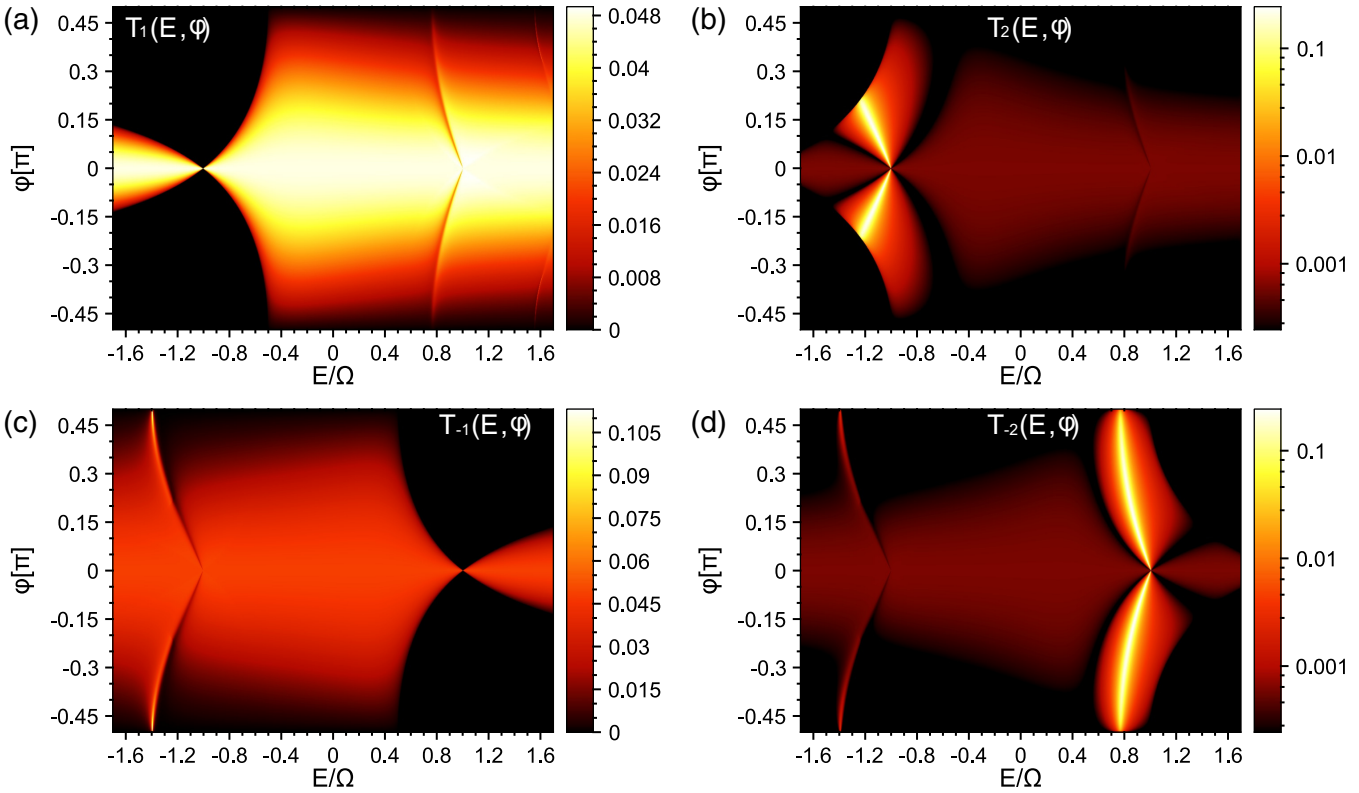

FIG. 7. Energy and incidence angle dependence of transmission probabilities for inelastic scattering to the sidebands. The static barrier strength is $Z_0 = 0.4\pi$ and the ac drive strength is $Z_1 = 0.45$.

$O(Z_1^2)$,

$$t_0 = t_0^{(0)} + Z_1^2\tau_0,$$
$$t_{\pm1} = Z_1\tau_{\pm1}, \tag{C3}$$
$$t_{\pm2} = Z_1^2\tau_{\pm2},$$

where we introduced for convenience $t_n^{(0)}(k_y,E) \equiv t^{(0)}(k_y,E_n)$. Keeping the same order of approximation in Eq. (C1) we can easily solve it with the following results,

$$\tau_0 = \left(\frac{1}{4} + t_0^{(0)}A_{0,1}\frac{A_{1,0}}{D_1} + t_0^{(0)}A_{0,-1}\frac{A_{-1,0}}{D_{-1}}\right)t_0^{(0)},$$
$$\tau_{\pm1} = -\frac{A_{\pm1,0}}{D_{\pm1}}t_0^{(0)}, \tag{C4}$$
$$\tau_{\pm2} = \left(\frac{A_{\pm2,\pm1}}{D_{\pm2}}\frac{A_{\pm1,0}}{D_{\pm1}} - \frac{A_{\pm2,0}}{D_{\pm2}}\right)t_0^{(0)},$$

which were also collected into Eq. (8). The transmission coefficients, Eq. (C3), supplemented by Eq. (C4) have a physically transparent form if they describe propagating waves, i.e., waves with all $E_n > |k_y|$. In this case we can identify $D_n^{-1} = t_n^{(0)}$ [see Eq. (B4)] and, reading the resulting expressions from right to left, we can distinguish the transmission processes depicted in Fig. 1(b) [except that $E_1 \neq E_b$ in the process (3), according to our assumption].

2. Close-to-resonance transmission

Now we will focus on the resonances associated with the case when the energy of one of the $n = \pm1$ sidebands hits the bound state, $E_{\pm1} = E_b$, and the corresponding channel is closed. They are observed as zeros in $T_{\pm1}$ and maxima in $T_{\pm2}$, dispersing with the incidence angle φ (see Fig. 2). For definiteness we will consider the resonance condition for $n = 1$, but this analysis is straightforward to repeat for $n = -1$. The resonance condition reads

$$D_1(k_y,E_r) = 0. \tag{C5}$$

We expand the D_1 coefficient in Eq. (C1) around the resonance energy assuming

$$E = E_b - \Omega + \delta E = E_r + \delta E, \quad |\delta E| \ll \{\Omega, |k_y|\},$$
$$D_1(k_y,E) \approx \frac{\delta E}{|k_y|\sin^2 Z_0}. \tag{C6}$$

Evaluating all other functions in Eqs. (C1) at $E = E_r$, we solve the resulting system of equations keeping only terms of order $O(\delta E, Z_1^2)$. The solution for t_0 and t_2 reads

$$t_0 = \frac{\delta E D_2 - Z_1^2 A_{1,2}A_{2,1}|k_y|\sin^2 Z_0}{\delta E D_0 D_2 - Z_1^2(D_2 A_{0,1}A_{1,0} + D_0 A_{1,2}A_{2,1})|k_y|\sin^2 Z_0}, \tag{C7}$$

$$t_2 = \frac{Z_1^2 A_{2,1}A_{1,0}|k_y|\sin^2 Z_0}{\delta E D_0 D_2 - Z_1^2(D_2 A_{0,1}A_{1,0} + D_0 A_{1,2}A_{2,1})|k_y|\sin^2 Z_0}. \tag{C8}$$

We note that for $|k_y| \to 0$, $|t_0|^2$ will be close to unity due to Klein tunneling [34] and there is no resonance behavior. If we consider the case when both the main channel $n = 0$ and

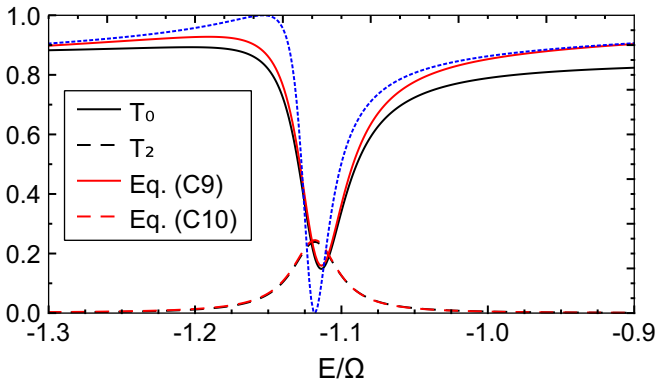

FIG. 8. Energy dependence of transmission probabilities T_0 and T_2 for incidence angle $\varphi = \pi/9$, $Z_0 = 0.4\pi$, and $Z_1 = 0.45$. The blue dotted line is the result for T_0 when neglecting scattering to the second sideband at E_2. In this case, the Fano resonance is fully developed (peak at unit transmission and dip at zero transmission).

the second sideband $n = 2$ are propagating, then Eqs. (C7) and (C8) can be rewritten as

$$t_0 = \frac{\delta E - Z_1^2 A_{1,2} t_2^{(0)} A_{2,1} |k_y| \sin^2 Z_0}{\delta E - Z_1^2 \left(t_0^{(0)} A_{0,1} A_{1,0} + A_{1,2} t_2^{(0)} A_{2,1}\right) |k_y| \sin^2 Z_0} t_0^{(0)}, \tag{C9}$$

$$t_2 = \frac{Z_1^2 A_{2,1} A_{1,0} t_0^{(0)} |k_y| \sin^2 Z_0}{\delta E - Z_1^2 \left(t_0^{(0)} A_{0,1} A_{1,0} + A_{1,2} t_2^{(0)} A_{2,1}\right) |k_y| \sin^2 Z_0} t_2^{(0)}, \tag{C10}$$

with the shorthand notation $t_0^{(0)} = t^{(0)}(E_r)$ and $t_2^{(0)} = t^{(0)}(E_r + 2\Omega)$. If we analyze these expressions we can see the following:

(1) if we compute the corresponding transmission probabilities, $T_0 = |t_0|^2$, and $T_2 = |t_2|^2$, we clearly see that T_0 has a Fano-type resonance shape, while T_2 is of Breit-Wigner type with the width of the resonances $\propto Z_1^2 |k_y| \sin^2 Z_0$;

(2) exactly at the resonance, $\delta E \to 0$, both t_0 and t_2 have finite values independent of Z_1 due to constructive interference between the first and the second sidebands.

In Fig. 8 we compare the approximate solution we have found with the exact numerical calculation [see inset of Fig. 2(b) in the main text]. We clearly see that Eqs. (C9) and (C10) correctly describe all the essential features of the transmission probabilities discussed above.

Finally, in a more strict expansion of all functions in Eq. (C1) to linear order in δE, more cumbersome expressions are obtained, but the above conclusions will not change, as also supported by the good agreement between the black and red lines in Fig. 8.

APPENDIX D: SCATTERING FIELD THEORY OF AC CURRENT

In this section we briefly describe the method we used to compute ac electric current. The theory below is valid as soon as a single-particle approach is justified, i.e., when particle-particle interactions can be neglected. Without loss of generality we assume particles incident on the barrier from the contact α [e.g., the source contact; see Fig. 1(a) in the main text]. Using the scattering basis, Eq. (A6), found above we construct a field operator

$$\hat{\Psi}_\alpha(x,y,t) = \int_{-\infty}^{+\infty} \frac{dk_y}{\sqrt{2\pi}} e^{ik_y y} \int_{|E|>|k_y|} \frac{dE}{\sqrt{2\pi}} \times e^{-iEt} [\hat{\gamma}_{\alpha,\text{in}}(k_y,E)\psi_\rightarrow(x,k_y,E) + \hat{\gamma}_{\alpha,\text{out}}(k_y,E)\psi_\leftarrow(x,k_y,E)] \tag{D1}$$

in the local coordinate system of the contact, where $\hat{\gamma}_{\alpha,\text{in/out}}(k_y,E)$ are the corresponding annihilation operators for the incoming/outgoing particles, which satisfy

$$\begin{aligned} \{\hat{\gamma}_{\alpha,\text{in}}(k_y,E), \hat{\gamma}^\dagger_{\beta,\text{in}}(k'_y,E')\} &= \delta_{\alpha,\beta}\delta(k_y - k'_y)\delta(E - E'), \\ \{\hat{\gamma}_{\alpha,\text{in}}(k_y,E), \hat{\gamma}_{\beta,\text{in}}(k'_y,E')\} &= 0, \\ \{\hat{\gamma}^\dagger_{\alpha,\text{in}}(k_y,E), \hat{\gamma}^\dagger_{\beta,\text{in}}(k'_y,E')\} &= 0. \end{aligned} \tag{D2}$$

According to the scattering theory the outgoing operator $\hat{\gamma}_{\alpha,\text{out}}(k_y,E)$ is, via a scattering matrix, related to the incoming one. For our case of an ac barrier and static contacts this relation reads

$$\hat{\gamma}_{\alpha,\text{out}}(k_y,E) = \sum_\beta \sum_{n,\text{propag.}} S_{\alpha\beta}(k_y;E,E_n)\hat{\gamma}_{\beta,\text{in}}(k_y,E_n), \tag{D3}$$

where we restrict the sum over sidebands to propagating waves only, which is equivalent to setting the scattering matrix elements to zero if an incoming/outgoing wave is evanescent. Then we construct the current operator defined by the standard expression [41]

$$\hat{I}_\alpha(x,t) = e \int dy\, \hat{\Psi}^\dagger_\alpha(x,y,t)\sigma_x\hat{\Psi}_\alpha(x,y,t), \tag{D4}$$

where e is the electron charge. Note that $\delta(k_y - k'_y)$ in Eq. (D2) must be understood in the sense of a Kronecker symbol meaning that we use Born–von Kármán periodic boundary conditions in the y direction. This means that there are correspondences

$$\delta(k_y - k'_y) = \int_{-\infty}^{+\infty} \frac{dy}{2\pi} e^{i(k_y - k'_y)y} \tag{D5}$$

$$\Leftrightarrow \frac{1}{L_y}\int_0^{L_y} dy\, e^{i(k_y^n - k_y^m)y} = \delta_{n,m} \tag{D6}$$

and

$$\frac{2\pi}{L_y}\sum_{k_y^n} \Leftrightarrow \int_{-\infty}^{+\infty} dk_y. \tag{D7}$$

To obtain an observable quantity $I_\alpha(x,t)$ we compute a statistical average of Eq. (D4) with the help of

$$\langle \hat{\gamma}^\dagger_{\alpha,\text{in}}(k_y,E)\hat{\gamma}_{\beta,\text{in}}(k_y,E')\rangle = \delta_{\alpha,\beta}\delta(E - E')f_\alpha(E), \tag{D8}$$

where $f_\alpha(E)$ is a Fermi-Dirac distribution in the contact α. The resulting expression has the form

$$I_\alpha(x,t) = \sum_{n=-\infty}^{+\infty} e^{-in\Omega t} I_{\alpha,n}(x), \quad I_{\alpha,-n}(x) = I^*_{\alpha,n}(x), \tag{D9}$$

where

$$I_{\alpha,n}(x) = e\int_{-\infty}^{+\infty} dk_y \int_{|E|>|k_y|} dE \Bigg\{ \delta_{n,0} f_\alpha(E) + \frac{\eta^*(k_y,E)+\bar{\eta}(k_y,E_n)}{2\sqrt{v(k_y,E)v(k_y,E_n)}} e^{-i[\kappa_x(k_y,E)+\kappa_x(k_y,E_n)]x} S_{\alpha\alpha}(k_y;E_n,E) f_\alpha(E)$$
$$+ \frac{\bar{\eta}^*(k_y,E_{-n})+\eta(k_y,E)}{2\sqrt{v(k_y,E_{-n})v(k_y,E)}} e^{i[\kappa_x(k_y,E_{-n})+\kappa_x(k_y,E)]x} [S_{\alpha\alpha}(k_y;E_{-n},E)]^\dagger f_\alpha(E)$$
$$+ \sum_\beta \sum_{m=-\infty}^{+\infty} \frac{\bar{\eta}^*(k_y,E)+\bar{\eta}(k_y,E_n)}{2\sqrt{v(k_y,E)v(k_y,E_n)}} e^{i[\kappa_x(k_y,E)-\kappa_x(k_y,E_n)]x} [S_{\alpha\beta}(k_y;E,E_m)]^\dagger S_{\alpha\beta}(k_y;E_n,E_m) f_\beta(E_m) \Bigg\}. \quad \text{(D10)}$$

Using unitarity of the scattering matrix [43],

$$\sum_\alpha \sum_n [S_{\alpha\beta}(k_y;E_n,E_m)]^\dagger S_{\alpha\gamma}(k_y;E_n,E) = \delta_{\beta,\gamma}\delta_{m,0}, \quad \text{(D11)}$$

$$\sum_\beta \sum_n S_{\gamma\beta}(k_y;E_m,E_n)[S_{\alpha\beta}(k_y;E,E_n)]^\dagger = \delta_{\alpha,\gamma}\delta_{m,0}, \quad \text{(D12)}$$

we can rewrite Eq. (D10) in the following form:

$$I_{\alpha,n}(x) = e\int_{-\infty}^{+\infty} dk_y \int_{|E|>|k_y|} dE \Bigg\{ \frac{\eta^*(k_y,E)+\bar{\eta}(k_y,E_n)}{2\sqrt{v(k_y,E)v(k_y,E_n)}} e^{-i[\kappa_x(k_y,E)+\kappa_x(k_y,E_n)]x} S_{\alpha\alpha}(k_y;E_n,E) f_\alpha(E)$$
$$+ \frac{\bar{\eta}^*(k_y,E_{-n})+\eta(k_y,E)}{2\sqrt{v(k_y,E_{-n})v(k_y,E)}} e^{i[\kappa_x(k_y,E_{-n})+\kappa_x(k_y,E)]x} [S_{\alpha\alpha}(k_y;E_{-n},E)]^\dagger f_\alpha(E) + \sum_\beta \sum_{m=-\infty}^{+\infty} \frac{\bar{\eta}^*(k_y,E_m)+\bar{\eta}(k_y,E_{n+m})}{2\sqrt{v(k_y,E_m)v(k_y,E_{n+m})}}$$
$$\times e^{i[\kappa_x(k_y,E_m)-\kappa_x(k_y,E_{n+m})]x} [S_{\alpha\beta}(k_y;E_m,E)]^\dagger S_{\alpha\beta}(k_y;E_{n+m},E)[f_\beta(E) - f_\alpha(E_m)] \Bigg\}. \quad \text{(D13)}$$

In contrast with the usual Büttiker theory [32], one cannot in general neglect the energy dependence of $\kappa_x(k_y,E)$ and $v(k_y,E_m)$ in Eq. (D13), because the Fermi energy E_F in graphene can be tuned to the Dirac point. On the other hand, if we keep the first two terms on the right-hand side of Eq. (D13), we see that the ac current components are formally determined by the full Fermi sea rather than states close to the Fermi surface only.

APPENDIX E: AC DIFFERENTIAL CONDUCTANCE

In this section we present formulas that we use to compute ac conductance for different sidebands in the main text. We assume that our system [see Fig. 1(a)] is at low temperature and compute a linear differential conductance with respect to the source-drain bias voltage V_S,

$$f_\alpha(E) = f(E - eV_\alpha), \quad -\frac{\partial f(E)}{\partial E} \to \delta(E - E_F),$$
$$G_n(E_F) = \left.\frac{\partial I_{D,n}(x=0^+,V_S)}{\partial V_S}\right|_{V_S\to 0}. \quad \text{(E1)}$$

Note that in principle the current, Eq. (D9), is a function of coordinate and we choose the point $x = 0^+$ in our calculations. If we use the results of the previous section we obtain

$$G_n(E_F) = \frac{e^2}{h}\int_{-\infty}^{\infty} dk_y \sum_{m=-\infty}^{+\infty} \frac{\eta^*(k_y,E_m)+\eta(k_y,E_{n+m})}{2\sqrt{v(k_y,E_m)v(k_y,E_{n+m})}}$$
$$\times\, t_m^\dagger(k_y,E) t_{n+m}(k_y,E)\Big|_{E=E_F}, \quad \text{(E2)}$$

where we have restored Planck's constant h to obtain the well-known conductance unit. This formula was used in Fig. 3. Finally, in Fig. 4 we present more details of the results obtained with the help of Eq. (E2) for sidebands with $n = \pm 1, \pm 2$.

[1] F. Schwierz, Graphene transistors, Nat. Nanotechnol. **5**, 487 (2010).

[2] T. Palacios, A. Hsu, and H. Wang, Applications of graphene devices in RF communications, IEEE Commun. Mag. **48**, 122 (2010).

[3] M. M. Glazov and S. D. Ganichev, High frequency electric field induced nonliear effects in graphene, Phys. Rep. **535**, 101 (2014).

[4] A. C. Ferrari, F. Bonaccorso, V. Fal'ko, K. S. Novoselov, S. Roche, P. Bøggild, S. Borini, F. H. L. Koppens, V. Palermo, N. Pugno *et al.*, Science and technology roadmap for graphene, related two-dimensional crystals, and hybrid systems, Nanoscale **7**, 4598 (2015).

[5] R. Cheng, J. Bai, L. Liao, H. Zhou, Y. Chen. L. Liu, Y.-C. Lin, S. Jiang, Y. Huang, and X. Duan, High-frequency self-aligned graphene transistors with transferred gate stacks, Proc. Natl. Acad. Sci. USA **109**, 11588 (2012).

[6] P. Rickhaus, P. Makk, M.-H. Liu, E. T'ov'ari, M. Weiss, R. Maurand. K. Richter, and C. Schönenberger, Snake trajectories in ultraclean graphene p-n junctions, Nat. Commun. **6**, 6470 (2015).

[7] P. Tassin, T. Koschny, and C. M. Soukoulis, Graphene for teraherz applications, Science **341**, 620 (2013).

[8] E. Prada, P. San-Jose, and H. Schomerus, Quantum pumping in graphene, Phys. Rev. B **80**, 245414 (2009).

[9] L. E. F. Foa Torres, H. L. Calvo, C. G. Rocha, and G. Cuniberti, Enhancing single-parameter quantum charge pumping in carbon-based devices, Appl. Phys. Lett. **99**, 092102 (2011).

[10] P. San-Jose, E. Prada, S. Kohler, and H. Schomerus, Single-parameter pumping in graphene, Phys. Rev. B **84**, 155408 (2011).

[11] P. San-Jose, E. Prada, H. Schomerus, and S. Kohler, Laser-induced quantum pumping in graphene, Appl. Phys. Lett. **101**, 153506 (2012).

[12] M. R. Connolly, K. L. Chiu, S. P. Giblin, M. Kataoka, J. D. Fletcher, C. Chua, J. P. Griffiths, G. A. C. Jones, V. I. Fal'ko, C. G. Smith, and T. J. B. M. Janssen, Gigahertz quantized charge pumping in graphene quantum dots, Nat. Nanotechnol. **8**, 417 (2013).

[13] S. A. Mikhailov and K. Ziegler, New Electromagnetic Mode in Graphene, Phys. Rev. Lett. **99**, 016803 (2007).

[14] S. A. Mikhailov and K. Ziegler, Nonlinear electromagnetic response of graphene: Frequency multiplication and the self-consistent field effects, J. Phys.: Condens. Matter **20**, 384204 (2008).

[15] S. V. Syzranov, M. V. Fistul, and K. B. Efetov Effect of radiation on transport in graphene, Phys. Rev. B **78**, 045407 (2008).

[16] H. L. Calvo, P. M. Perez-Piskunow, S. Roche, and L. E. F. Foa Torress, Laser-induced effects on the electronic features of graphene nanoribbons, Appl. Phys. Lett. **101**, 253506 (2012).

[17] I. Al-Naib, J. E. Sipe, and M. M. Dignam, High harmonic generation in undoped graphene: Interplay of inter- and intraband dynamics, Phys. Rev. B **90**, 245423 (2014).

[18] C. Sinha and R. Biswas, Transmission of electron through monolayer graphene laser barrier, Appl. Phys. Lett. **100**, 183107 (2012).

[19] B. Trauzettel, Ya. M. Blanter, and A. F. Morpurgo, Photon-assisted electron transport in graphene: Scattering theory analysis, Phys. Rev. B **75**, 035305 (2007).

[20] M. A. Zeb, K. Sabeeh, and M. Tahir, Chiral tunneling through a time-periodic potential in monolayer graphene, Phys. Rev. B **78**, 165420 (2008).

[21] C. G. Rocha, L. E. F. Foa Torres, and G. Cuniberti, ac transport in graphene-based Fabry-Pérot devices, Phys. Rev. B **81**, 115435 (2010).

[22] S. E. Savel'ev, W. Häusler, and P. Hänggi, Current Resonances in Graphene with Time-Dependent Potential Barriers, Phys. Rev. Lett. **109**, 226602 (2012).

[23] W. T. Lu, S.-J. Wang, W. Li, Y.-L. Wang, and C.-Z. Ye, Fano-type resonance through a time-periodic potential in graphene, J. Appl. Phys. **111**, 103717 (2012).

[24] L. Z. Szabó, M. G. Benedict, A. Czirják, and P. Földi, Relativistic electron transport through an oscillating barrier: Wave-packet generation and Fano-type resonances, Phys. Rev. B **88**, 075438 (2013).

[25] R. Zhu, J.-H. Dai, and Y. Gao, Fano resonance in the nonadiabatically pumped shot noise of a time-dependent quantum well in two-dimensional electron gas and graphene, J. Appl. Phys. **117**, 164306 (2015).

[26] P. F. Bagwell and R. K. Lake, Resonances in transmission through an oscillating barrier, Phys. Rev. B **46**, 15329 (1992).

[27] M. H. Pedersen and M. Büttiker, Scattering theory of photon-assisted electron transport, Phys. Rev. B **58**, 12993 (1998).

[28] G. Platero and R. Aguado, Photon-assisted transport in semiconductor nanostructures, Phys. Rep. **395**, 1 (2004).

[29] S. Kohler, J. Lehmann, and P. Hänggi, Driven quantum transport on the nanoscale, Phys. Rep. **406**, 379 (2005).

[30] A. E. Miroshnichenko, S. Flach, and Yu. S. Kivshar, Fano resonances in nanoscale structures, Rev. Mod. Phys. **82**, 2257 (2010).

[31] J. Tworzydlo, B. Trauzettel, M. Titov, A. Rycerz, and C. W. J. Beenakker, Sub-Poissonian Shot Noise in Graphene, Phys. Rev. Lett. **96**, 246802 (2006).

[32] Ya. M. Blanter and M. Büttiker, Shot noise in mesoscopic conductors, Phys. Rep. **336**, 1 (2000).

[33] B. H. J. McKellar and G. J. Stephenson, Jr., Klein paradox and the Dirac-Kronig-Penney model, Phys. Rev. A **36**, 2566 (1987).

[34] M. I. Katsnelson, K. S. Novoselov, and A. K. Geim, Chiral tunneling and the Klein paradox in graphene, Nat. Phys. **2**, 620 (2006).

[35] S. Rosenblatt. H. Lin, V. Sazonova, S. Tiwari, and P. L. McEuen, Mixing at 50 GHz using a single-walled carbon nanotube transistor, Appl. Phys. Lett. **87**, 153111 (2005).

[36] L. Liao, J. Bai, R. Cheng, H. Zhou, L. Liu, Y. Liu, Y. Huang, and X. Duan, Scalable fabrication of self-aligned graphene transistors and circuits on glass, Nano Lett. **12**, 2653 (2011).

[37] K. S. Novoselov, Z. Jiang, Y. Zhang, S. V. Morozov, H. L. Stormer, U. Zeitler, J. C. Maan, G. S. Boebinger, P. Kim, and A. K. Geim, Room-temperature quantum Hall effect in graphene, Science **315**, 1379 (2007).

[38] W. Li and L. E. Reichl, Floquet scattering through a time-periodic potential, Phys. Rev. B **60**, 15732 (1999).

[39] M. I. Katsnelson, *Graphene: Carbon in Two Dimensions* (Cambridge University Press, United Kingdom, 2012).

[40] L. E. F. Foa Torres, S. Roche, and J.-C. Charlier, *Introduction to Graphene-Based Nanomaterials* (Cambridge University Press, United Kingdom, 2014).

[41] M. Büttiker, Scattering theory of current and intensity noise correlations in conductors and waveguides, Phys. Rev. B **46**, 12485 (1992).

[42] J. R. Taylor, *Scattering Theory: The Quantum Theory of Nonrelativistic Collisions* (Dover Publications, New York, 2006).

[43] M. Moskalets and M. Büttiker, Adiabatic quantum pump in the presence of external ac voltages, Phys. Rev. B **69**, 205316 (2004).